SEMARAK ILMU PUBLISHING

Journal of Advanced Research in Numerical Heat Transfer

Journal homepage:
https://semarakilmu.com.my/journals/index.php/arnht/index
ISSN: 2735-0142

Simulation of Dissimilar (Al1100-Cu) Friction Stir Welding Using Convection Coefficient Between Workpiece and Backing Plate Based on Its Deformation

Fathi Robbany[1,*], Djarot Bangun Darmadi[1], Yudy Surya Irawan[1], Moch. Agus Choiron[1], Widia Setiawan[2], Marco Talice[3]

[1] Department of Mechanical Engineering, University of Brawijaya, Malang, Indonesia
[2] Department of Mechanical Engineering, Vocational College Gadjah Mada University, Yogyakarta, Indonesia
[3] PMSQUARED ENGINEERING S.r.l.s., Cagliari, Italy

ARTICLE INFO

Article history:
Received 21 July 2024
Received in revised form 23 August 2024
Accepted 20 September 2024
Available online 30 October 2024

Keywords:
Computational fluid dynamics; Dissimilar; Friction stir welding; Modeling

ABSTRACT

Friction stir welding is considered a solution to conventional welding issues, particularly when dissimilar materials are involved. The implication of complex phenomena encourages researchers to utilize numerical simulations in their research. Despite the backing plate being the most significant cause of heat loss, researchers tend to simplify the heat transfer coefficient for the backing plate without considering the workpiece deformation pattern. The applied pressure by the tool increases the contact conductance between the workpiece and the backing plate, influencing heat transfer coefficient distribution. This paper aims to model the FSW process involving workpiece deformation and compare it with uniform and temperature dependent in existing models. A backing plate in the form of asbestos is employed to capture the workpiece deformation on an experimental test. Quadratic polynomial equations are used as an approach to measure deformation patterns. Based on the results of this study, the workpiece yield strength and the tool axial force play crucial roles in determining the convection coefficient. This is proven by the convection coefficient distribution based on the deformation pattern, which produced a temperature history closer to the experimental results than uniform and temperature based. Higher temperatures on the advancing side apply to areas close to the tool, and the material's thermal conductivity becomes more decisive as the distance increases. In connection with material flow, despite a flat tool being used, the material on the advancing side tends to be extruded upward and downward on the retreating side perpendicular to the tool. Validation of material flow in the model was also carried out.

1. Introduction

The growing interest in joining dissimilar materials in recent times [1] is inseparable from the possibility of exploiting the prominent properties of the materials to be combined [2], low operational and material costs, design flexibility, and the ability to enhance the electrical and

* *Corresponding author.*
E-mail address: fathirobbany@gmail.com (Fathi Robbany)

https://doi.org/10.37934/arnht.25.1.3752

mechanical properties [3] of the product. The combination of aluminum and copper (Al-Cu) is an example of a commonly used material in the electrical industry [4]. The dissimilar Al-Cu is widely used for battery cells in electric cars for its high electrical conductivity and good mechanical properties [5]. However, joining Al-Cu beyond its melting point will cause the formation of intermetallic compounds, resulting in poor joint quality [6]. Low heat input in friction stir welding (FSW) allows joining material without transcending its melting point so that the formation of the intermetallic phase can be controlled, simultaneously increasing joint mechanical properties [7].

The FSW process is essentially like combining two pieces of clay through the use of heat by friction to produce a nugget zone [8]. Though the concept appears simple, the phenomenon behind it is very complex [9], consisting of a nonlinear and strong relationship between temperature and material flow. To understand its process in depth, observations and measurements must be made while welding is in progress or can also be done using numerical simulations [10]. Considering costs, research time, and emerging complex phenomena [11,12], many welding studies are carried out using numerical simulations. Knowing all the fundamental processes involved in detail is essential in producing high strength and defect-free welded joints [13].

Many efforts have been made using numerical simulations in the FSW process, which are in good agreement with experimental validation, especially in the thermal field. Although the contact between the workpiece and the backing plate is responsible for most of the heat loss from the workpiece through conduction [14], authors tend to simplify the conduction as convection with a uniformly high magnitude of convection coefficient [15] or depend only on temperature [16]. In fact, it is known that the thermal contact conductance found at the workpiece-backing plate interface is a function of several dominant parameters, namely, material properties, surface geometry, workpiece temperature, pressure, and filling fluid [17]. This indicates that the influence of the backing plate has not received as much attention as other parameters, such as tool design, welding speed, and other parameter processes [18].

When two flat objects make contact, geometrical imperfections on the two surfaces cause them to stick together only at specific points, as shown in Figure 1. This contact is never thermally perfect, giving rise to thermal contact resistance between layers [19]. When pressure between objects increases, the peak of surface roughness starts to deform and creates a path for the heat flux to flow by conduction [20]. In atmospheric conditions, heat transfer across the contact interface consists of conduction through the air gap, radiation from the walls, and conduction at the contact point [21]. Hence, deformation due to applied pressure by the tool in the FSW process will affect heat loss through conduction to the backing plate.

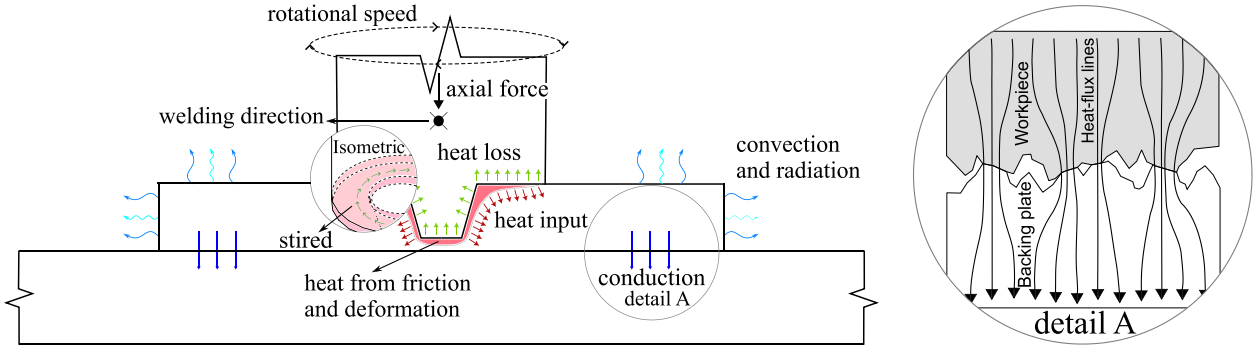

Fig. 1. FSW scheme and contact conduction between the workpiece and the backing plate

Axial force and backing plate significantly influence the final weld properties [22]. The greater the axial force, the greater the contact conductance [21] due to the surface roughness peak deformation, thus creating a conduction path. Using backing plates with high thermal diffusivity, such as copper,

causes void defects due to excessive heat extraction [23]. The temperature in the stir zone must be maintained high enough. Thus, a backing plate with high thermal diffusivity can also be used in welding at a low traverse speed [18]. Those settings result in lower energy efficiency and productivity for certain power limits as a consequence [24]. On the other hand, Imam *et al.*, [25] use a backing plate with low thermal diffusivity (asbestos) to produce defect-free welds on the butt and lap joints. However, low thermal diffusivity at high rotational tool speeds and low traverse speeds can cause flash defects [26].

Based on the literature review, no previous simulation study has considered deformation patterns to determine the distribution of convection coefficients at the interface between the workpiece and the backing plate. Therefore, this research aims to develop numerical simulations to determine the distribution of convection coefficients at the bottom of the workpiece on commercial pure aluminum (Al1100) and commercial pure copper (Cu) materials based on their deformation. To simulate thermomechanical phenomena in the FSW process, the computational fluid dynamics (CFD) approach was chosen because it has proven to be the most accurate of all simulation procedures in FSW modeling [27]. Validation was carried out on the temperature history between numerical simulations with six thermocouples in experimental results, and validation of the Al1100-Cu mixture traces from the front and top views was also performed. Hopefully, the FSW simulation's cooling rate due to conduction from the workpiece to the backing plate will resemble the actual phenomenon. Thus, it can be beneficial to control peak temperature [22], defect [25], hardness [28], and strength [29] of the joint.

2. Experimental Procedure

Two dissimilar plates of Al1100 and Cu with dimensions of 200×75×3 mm were joined with FSW unidirectional using a side of 200 mm. Six thermocouples were installed on the workpiece as temperature history recorders with a distance of 15 mm between each thermocouple and 15 mm from the meeting point between Al1100 and Cu. In Al-Cu welding, almost all researchers recommend placing Cu material on the retreating side [30]. Likewise, in this study, Al1100 was placed on the advancing side (AS) while Cu was on the retreating side (RS).

Tools made of EMS 45 were used, with a radius of 10 and 2 mm for the shoulder (R_s) and pin (R_p), respectively, and 2.2 mm for the pin height (H_p). The tool constantly rotates and moves with a rotational speed (ω) of 2280 rpm and a welding speed (U) of 1 mm/s. Shankar *et al.*, reveal that tool offset on harder materials shows a dominant effect [31]. Hence, the tool was shifted by 0.5 mm to the Cu side in this study.

This research focused on determining the distribution of convection coefficients based on the workpiece's deformation. Five mm thick asbestos was used as a backing plate to capture the formed bending line, as it is relatively soft but firm enough to hold the workpiece. Its schematic can be seen in Figure 2(a). A quadratic polynomial was used to approximate bending line measurements as in Figure 2(b) and as a distribution reference for the convection coefficient on the bottom of the workpiece.

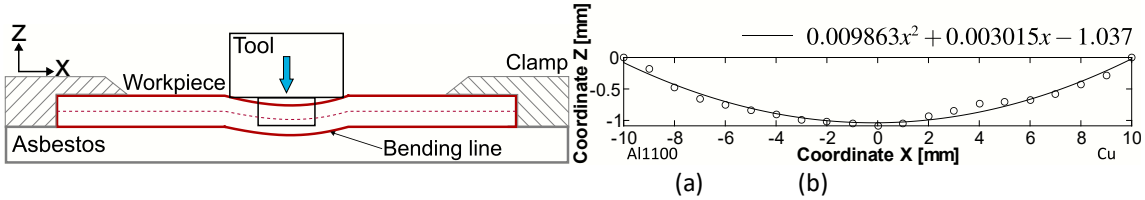

Fig. 2. Bending line in (a) scheme and (b) measurement result

3. Numerical Simulation Procedure

3.1 Assumptions

Thermal and material flow models were developed using ANSYS Fluent software, where heat and mass transfer equations were solved simultaneously. The volume of fluid method (VOF) was chosen to imitate dissimilar material behavior, which was based on the small diffusion coefficient between aluminum and copper and the short welding time. The workpiece material was considered a non-Newtonian, incompressible, immiscible, and viscoplastic fluid. The viscosity (μ) model was approached based on the formulation of flow stress (σ_s) and effective strain rate ($\bar{\dot{\varepsilon}}$), as in Eqs. (1-4) [32].

$$\sigma_s = \frac{1}{\alpha}\ln\left\{\left(\frac{Z}{A}\right)^{1/n} + \left[\left(\frac{Z}{A}\right)^{2/n} + 1\right]^{1/2}\right\} \tag{1}$$

$$Z(T, \bar{\dot{\varepsilon}}) = \bar{\dot{\varepsilon}} \exp\left(\frac{Q}{RT}\right) \tag{2}$$

$$\bar{\dot{\varepsilon}} = \sqrt{\frac{2}{3}\left[\frac{1}{2}\left(\frac{\partial u_i}{\partial x_j} + \frac{\partial u_j}{\partial x_i}\right)\right]^2} \tag{3}$$

$$\mu = \frac{\sigma_s}{3\bar{\dot{\varepsilon}}} \tag{4}$$

where Z is the Zener-Hollomon parameter, Q and R are temperature independent activation energy and gas constant, while α, A, and n are material constants. The velocity of plastic flow is denoted by u with i,j = 1, 2, and 3, representing X, Y, and Z directions.

2.1 Boundary Conditions and Mesh

In the experiment, the surface of the workpiece becomes curved due to tool pressure during welding. However, for simplicity and computational stability, the curved surface of the workpiece is assumed to be flat. Cartesian coordinates in 3D are used with the datum at the bottom of the workpiece parallel to the tool center point. Since the shoulder penetration depth influences material flow and heat generation [33], the shoulder penetration depth was also considered in the model, as shown in Figure 3. Following the experimental conditions, the shoulder penetration depth was set to 0.3 mm.

The asymmetrically shaped mesh tends to cause asymmetrical material flow distribution [33]. The mesh is modified to be symmetrical to eliminate this possibility, as shown in Figure 4. In CFD modeling, accuracy, reliability, and computation time are the main considerations [34]. To more accurately capture the calculated gradient without significantly increasing computation time, a smaller mesh was placed near the workpiece-tool interface, and a larger one was used far from the shear zone.

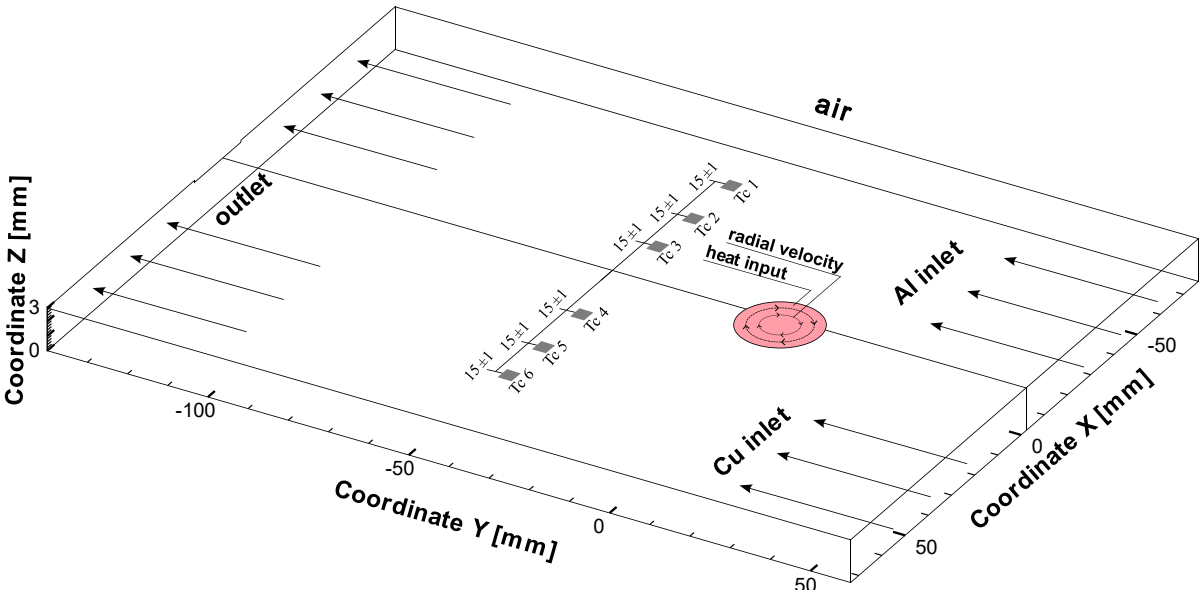

Fig. 3. Boundary conditions in the numerical simulation

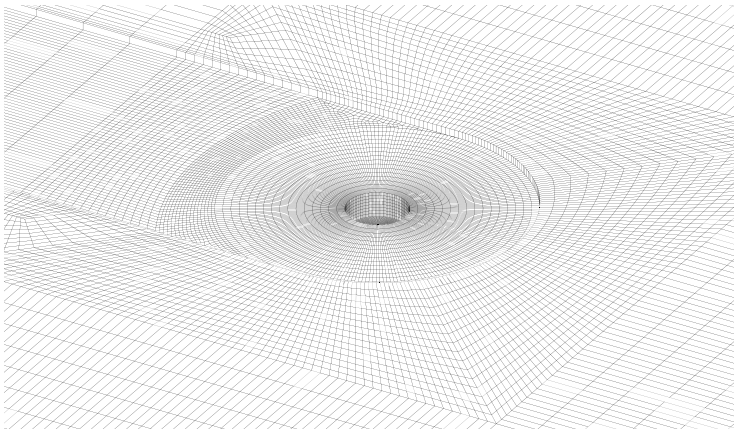

Fig. 4. Mesh in the numerical simulation

At the workpiece-tool interface, heat input loads and radial velocity were applied. The heat input total as a result of friction and material deformation was calculated by Eq. (5), and the fraction of heat that flowed to the workpiece follows Eq. (6) [35].

$$q(r) = \left[(1-\delta)\eta\frac{\sigma_y}{\sqrt{3}} + \delta\mu_f P_N\right]\left(\frac{2\pi\omega}{60}r - U\sin\theta\right) \tag{5}$$

$$q(r)_w = \frac{\sqrt{k_w\rho_w C_{p_w}}}{\sqrt{k_w\rho_w C_{p_w}}+\sqrt{k_T\rho_T C_{p_T}}}\, q(r) \tag{6}$$

with δ representing slip rate, P_N is axial downward pressure, μ_f is the friction coefficient on the workpiece-tool interfaces, σ_y is workpiece yield strength, and η is the efficiency of plastic deformation work. Thermal conductivity is denoted as k, heat capacity as C_p, and density as ρ. Subscripts $W$and Trepresent the workpiece and tool, respectively.

The velocity load for each component follows the equation Eq. (7) and Eq. (8) [35]. At the same time, the slip rate and dynamic friction coefficient model in this study are computed by Eq. (9) and Eq. (10) [36].

$$u_x = (1-\delta)\frac{2\pi\omega}{60} r\cos\theta \tag{7}$$

$$u_y = (1-\delta)\frac{2\pi\omega}{60} r\sin\theta - U \tag{8}$$

$$\delta = 1 - \exp\left(-\frac{1}{\delta_0}\frac{\omega}{\omega_0}\frac{r}{R_s}\right) \tag{9}$$

$$\mu_f = \mu_{f0}\exp\left(-\lambda\delta\frac{2\pi\omega}{60} r\right) \tag{10}$$

where δ_0 and λ are constants, and ω_0 is a constant to nondimensionalize rotational speed of the tool. The values of δ_0 and λ were taken as 0.4 and 1 s/m, respectively.

In dissimilar welding, Eq. (6) becomes more complex because the volume fraction between Al1100 and Cu is decisive. A higher Al1100 fraction will result in a lower fraction of heat going to the workpiece and vice versa. The same thing also happens as the temperature of the workpiece increases. In simple terms, the fraction of heat going to the workpiece can be seen in Figure 5.

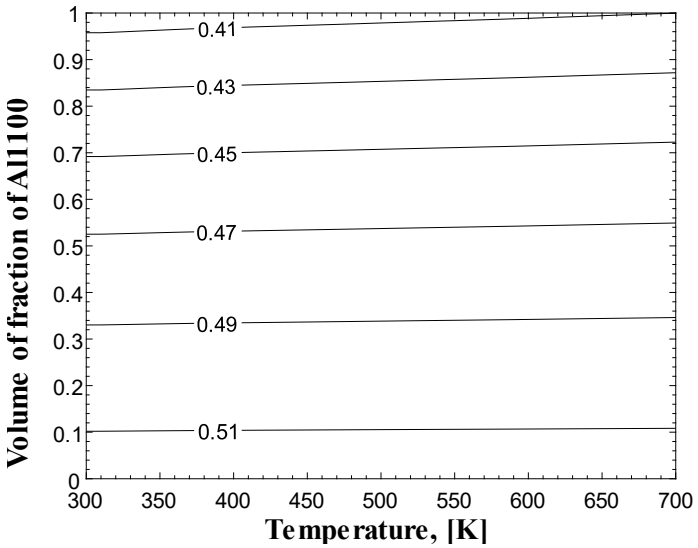

Fig. 5. Heat fraction flowing to the workpiece based on VOF of Al1100 and temperature

The heat that flows into the workpiece will be dissipated through convection, radiation, and conduction. The equation of convection and radiation on any surface of the workpiece that is in contact with air follows Eq. (11). However, conduction at the bottom of the workpiece due to intimate contact with the backing plate, is only applied by convection, which follows Eq. (12).

$$k\frac{\partial T}{\partial z} = \sigma_r\varepsilon_r(\mathrm{T}^4 - T_a^4) + h_t(T - T_a) \tag{11}$$

$$k\frac{\partial T}{\partial z} = h_b \times (T - T_a) \tag{12}$$

where σ_r is the Stefan-Boltzmann constant, ε_r is the external emissivity, T_a is the ambient temperature, and h_t and h_b are the convective heat transfer coefficient at the top and bottom surface of the workpiece. All physical properties used in this research are summarized in Table 1. Note that material properties dependent on temperature, including thermal conductivity, heat

capacity, and yield strength in Al1100 and Cu, are not presented as specific numerical values. Instead, these properties follow the given reference.

Table 1
The physical properties of all parts

Material	Al1100	Cu	EMS 45	Units
Density	2710	8940	7850	kg/m^3
Thermal conductivity	[30]	[31]	17.879	W/m-K
Heat capacity	[30]	[31]	554.2	J/kg-K
Yield strength	[32]	[31]	-	MPa
Q	158.3e3	208e3	-	kJ/mol
n	5.66	7.946	-	-
A	5.17e10	1.95e12	-	s^{-1}
α	0.045e-6	0.012e-6	-	MPa^{-1}
Boundary viscosity	1e6	1e6	-	Pa·s
μ_{f0}	0.4	0.32	-	-
ω_0	50	40	-	rpm
h_t	30	13	-	W/m^{2}K
External emissivity	0.86	0.04	-	-

There are three variations in the convection coefficient distribution on the bottom of the workpiece, namely uniform (Eq. (13)), based on temperature (Eq. (14) [16]) as seen in Figure 6(a), and also based on the workpiece deformation (Eq. (15)), which can be seen in Figure 6(b).

$$h_{bu} = 120\ W/m^2K \tag{13}$$

$$h_{bt} = h_{b0} \times (T - T_a)^{0.25} \times \frac{h_{bu} \times A_w}{\sum_{i=1}^{Total\ face} h_{bi} \times A_i} \tag{14}$$

$$h_{bd} = \begin{cases} h_{b0}(P_1 x^2 + P_2 x + P_3), & r \le R_s \\ 94\ W/m^2K, & r > R_s \end{cases} \tag{15}$$

where h_{b0} is an adjustment factor constant, *i* denotes the wall face number in Fluent, and A_w is the total bottom area of the workpiece. P_1, P_2, and P_3 are equal to 0.009863, 0.003015, and -1.037, respectively. The total value ($h_b \times A_w$) of the three variations is kept the same (3.6 W/K).

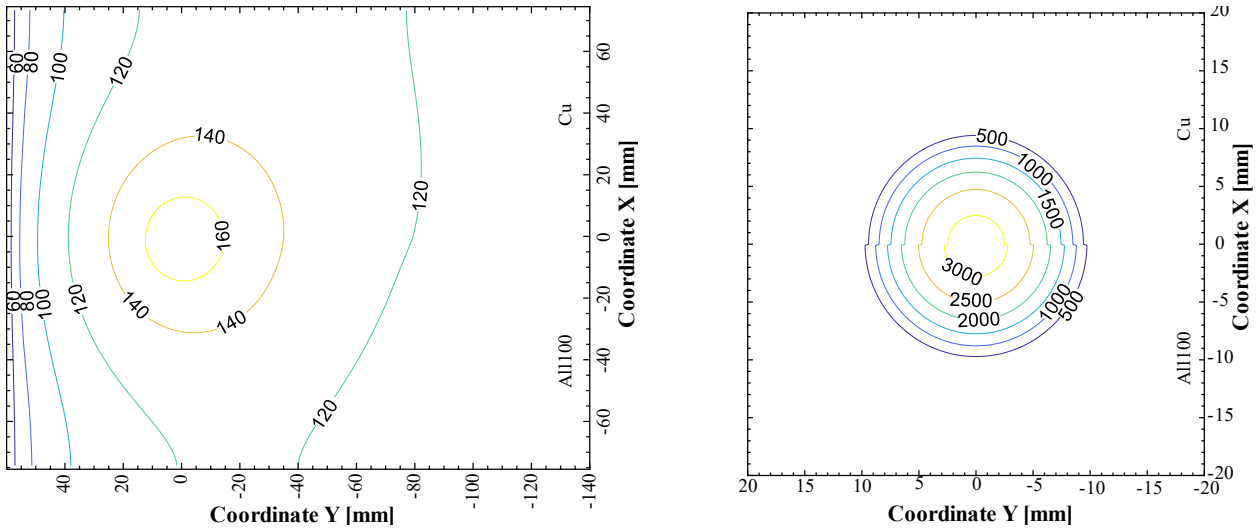

(a) (b)

Fig. 6. Distribution of convection coefficient at the bottom of the workpiece (h_b) for (a) temperature dependent and (b) deformation dependent

It is important to note that using the trial-and-error method, all three approaches will show results close to the experiment. Therefore, it must be emphasized that the backing plate in this study employs asbestos, known as a heat insulator. So, the distribution of the convection coefficient, which produces the slightest difference between simulation and experiments with the minimum average, is the most reasonable approach.

4. Results and Discussion

The material was cut using ASTM E8 [37] standards with subsize sizes using an electrical discharge machining (EDM). The thickness in the joint area (below the tool) is 2.7 mm. The ultimate tensile strength (UTS) has a value of 54.1 MPa. The aforementioned local pressure of the tool causes deformation at the peak surface roughness of the workpiece-backing plate interface. Figure 7 shows that the surface condition becomes rougher, especially on the path the tool passes. This argument is corroborated by surface roughness measurements at several locations for R_a, R_z, and R_q, which are shown in Table 2. The intimate contact that occurs creates conduction heat flux that is concentrated at the bottom of the tool.

Fig. 7. Arbitrary magnification at the joint bottom view

Table 2
Surface roughness measurements based on the distance at the Al1100-Cu intersection

From center	Al1100 [μm]			Cu [μm]		
	R_a	R_z	R_q	R_a	R_z	R_q
3 mm	10.16	45.45	12.13	6.24	31.4	7.94
6 mm	8.52	43.62	10.46	5.46	24.42	6.48
9 mm	6.48	34.48	8.06	3.59	18.48	4.47
Base	0.61	5.59	0.78	0.47	3.97	0.61

4.1 Temperature History

The comparison of the temperature history between the thermocouple in the experiment and the simulation results for the Al1100 part is shown in Figure 8, and the Cu part is shown in Figure 9. Figure 8(a-c) and Figure 9(a-c), respectively, are graphs for uniform distribution (h_{bu}), temperature dependent (h_{bt}), and deformation dependent (h_{bd}) of the convection coefficient. The measurement point is adjusted to the placement of the thermocouple, as in Figure 3, and at the mid-thickness of the workpiece. In this research, steady-state modeling was carried out so that the time for the simulation readings was approximated by $t = U/y_s$. Where t is time, and Y_s is the Y coordinate from minimum to maximum value.

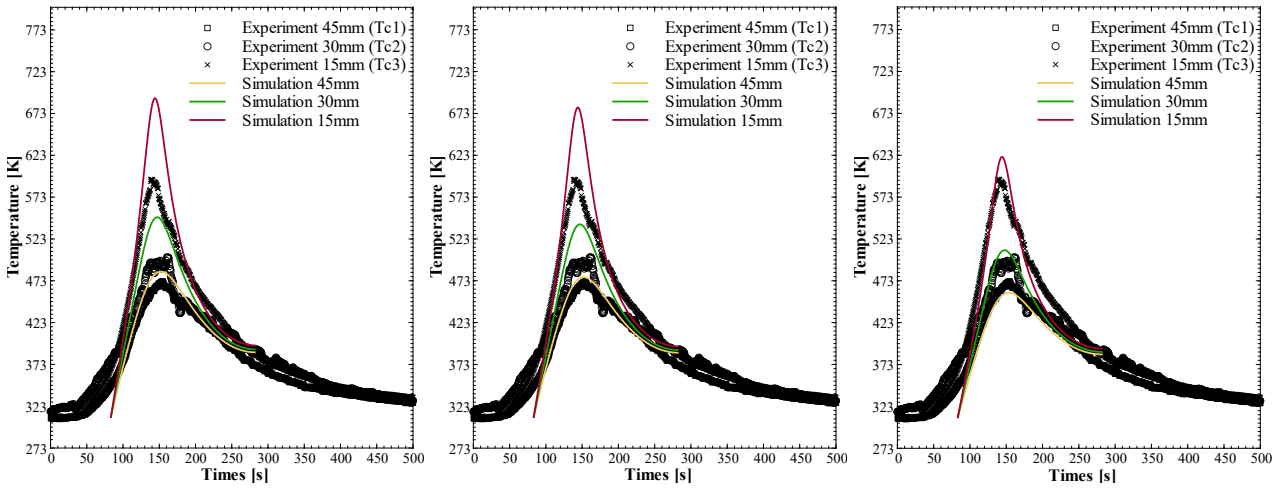

Fig. 8. Temperature history of Al1100 for (a) h_{bu}; (b) h_{bt} and; (c) h_{bd}

As we can see in Figure 8(a-c) and Figure 9(a-c), h_{bu} tends to produce predictions of temperatures that are much higher than experiments, likewise with h_{bt}, although it is slightly closer. By carrying out a concentrated distribution based on the deformation pattern, the temperature prediction is very close to the experiment compared to the other two approaches. This is because h_{bu} and h_{bt} does not consider the workpiece's curvature due to tool pressure. So, the simulation result tends to overpredict the peak temperature. By considering the curvature of the workpiece, h_b will be concentrated at the bottom of the tool. Hence, the heat lost to the backing plate through conduction will be higher, even with the same amount of $h_b \times A_w$.

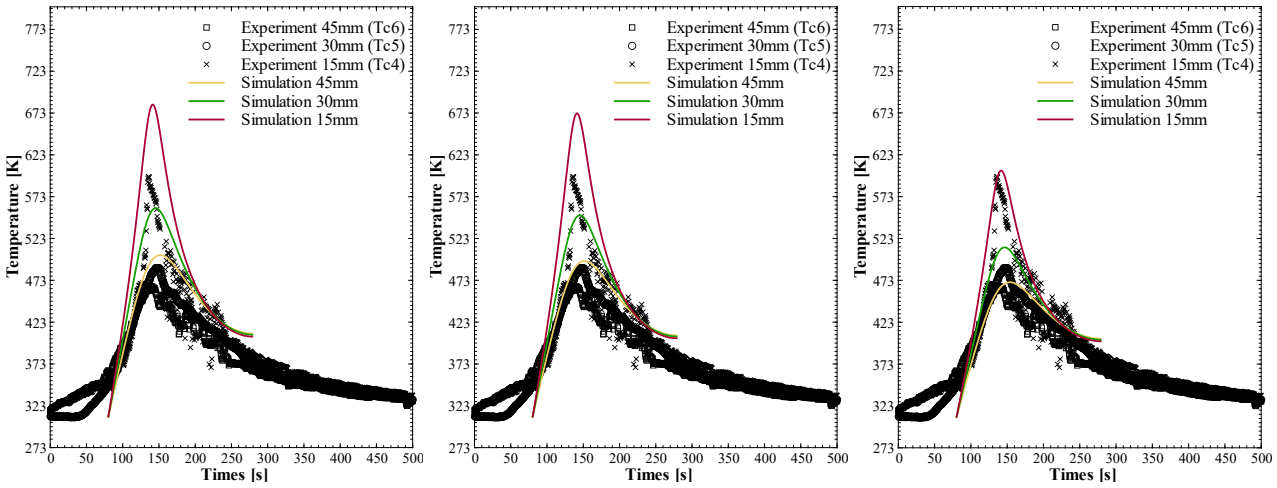

Fig. 9. Temperature history of Cu for (a) h_{bu}; (b) h_{bt} and; (c) h_{bd}

By combining the results from Al1100 and Cu on the deformation dependent approach because it is proven to produce the closest temperature predictions. The Al100 side (AS) has a higher peak temperature compared to the Cu side (RS). This situation applies to areas adjacent to the tool, such as at a distance of 15 mm from the tool axis, as shown in Figure 10(a). This is because the relative speed of the AS is higher than the RS, so the heat entering due to friction is higher.

In the same picture (Figure 10(a)), the RS has a higher peak temperature at a longer distance (30 and 45 mm) from the tool. This is because material properties have a more dominant effect as the distance to the tool/heat source increases. Material thermal properties, especially thermal conductivity, determine the temperature distribution of a welding process [38]. Because Cu's thermal conductivity is higher than Al1100's, heat tends to flow to the RS. This can be proven in the temperature contour plot, which can be seen in Figure 10(b). Thus, it can be concluded that the temperature asymmetry in dissimilar welding is a result of the relative speed of the tool between the AS and the RS and the differences in material properties of the two.

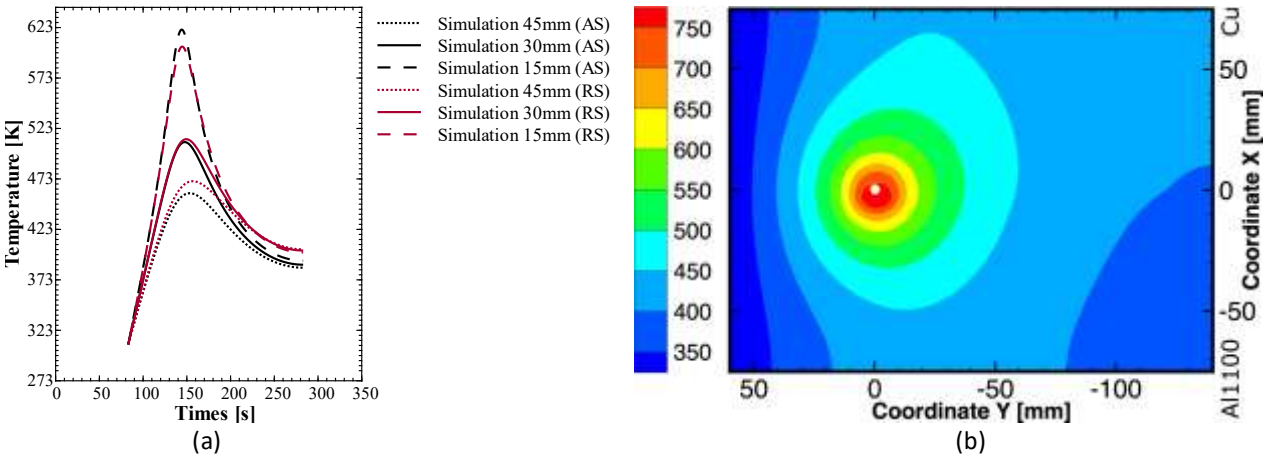

Fig. 10. Temperature on the AS and the RS side on (a) history and (b) contour plot

4.2 Material Flow

The tool's forward and rotary movement causes the material at the front to be extruded towards the back of the tool within each rotation. Figure 11(a) shows that the movement of material starts at AS (point A), begins to move in a circle pattern, and is then stacked with the area above (point B),

and so on, until it reaches the RS section (point F). These results are in line with experimental research conducted by Jagadeesha [39]. By using markers scattered in several places, they concluded that the material in the AS rotated almost 360° before settling on the rear AS, as seen in Figure 11(b).

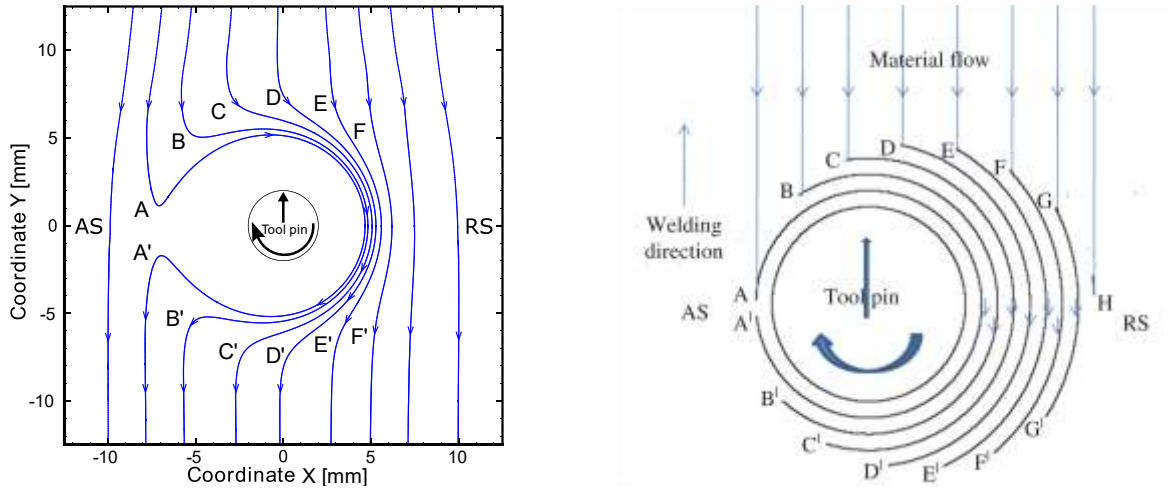

(a) (b)

Fig. 11. Material flow for (a) simulation at Z = 2.5 mm and (b) result by Jagaadesha [39]

If we display the streamline entirely in 3D, as in Figure 12 (a), there are streamlines form a complete circle due to the wall's no-slip condition, which represents the interface between the workpiece and the tool. This result is reinforced by experimental conditions where some of the material is stuck to the tool interface both on the shoulder and pin, as shown in Figure 13 (a). Streamline coloring based on velocity magnitude in Figure 12 (a) also indicates that the material is deformed more (faster) in the area close to the pin.

The streamline plot coloring based on density in Figure 12 (b) shows that the tool tends to only push material from the AS towards the RS. Only a small portion of material mixing (stirred) of the material at the top near the shoulder. The same thing was also expressed by Colligan [40] and Krishnan [41], that not everything that is deformed by the pin undergoes “stirred” processing; there is very little material mixing of the material in the FSW process, and there were more amounts of “stirring” near the top.

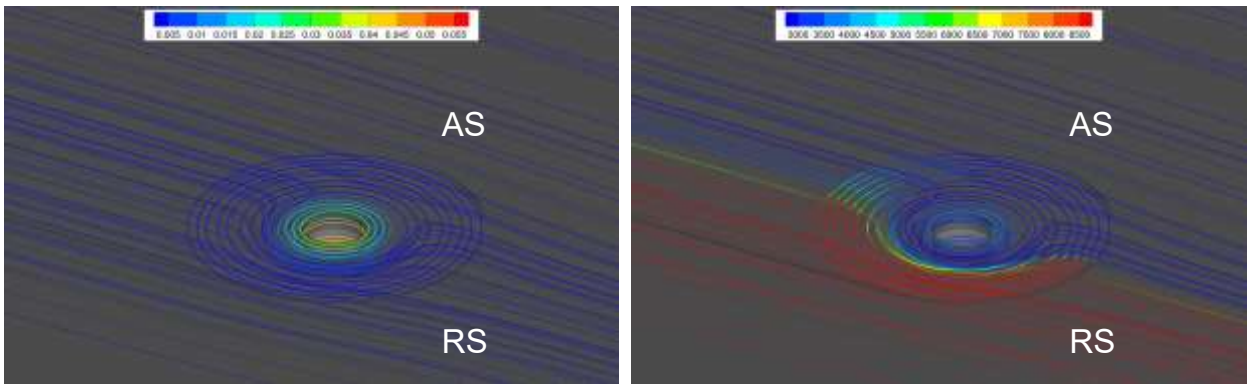

(a) (b)

Fig. 12. Material flow in 3D for (a) colored by velocity magnitude and (b) colored by density

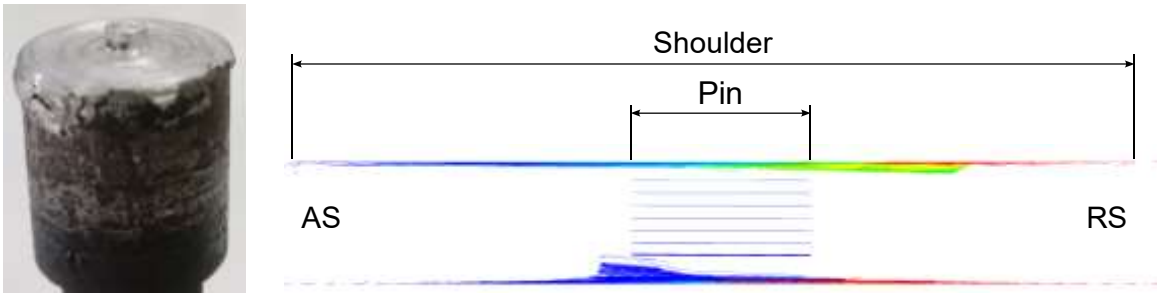

(a) b)

Fig. 13. (a) workpiece material residue at the tool interface and (b) material flow in simulation at Y = 0 mm (XZ plane) colored by its density

Figure 13 (b) shows that although non-threaded pins are used, the material will be extruded vertically up and down. When material is carried from the AS to the RS side, it causes the RS side to become denser, thus tending to extrude material from the leading edge (LE) downwards. On the other hand, the top of the RS side becomes less dense, so it tends to extrude material from LE upwards with the help of tool axial pressure. This trend is validated with the experimental and numerical simulation results at the front view (XZ plane) shown in Figure 14 (a) and Figure 14 (b).

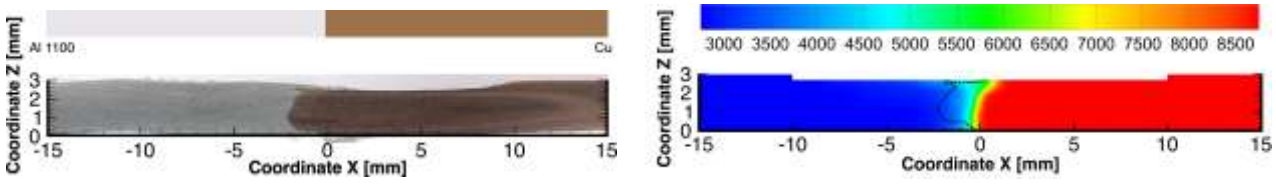

(a) (b)

Fig. 14. Front view (XZ plane) results at Y = -40 mm for (a) experiment and (b) simulation which is colored by density

The material flow is also validated with the experimental results on top view (XY plane) shown in Figure 15(a) and Figure 15(b) for each experiment and simulation result. Even though there are differences between experiment and simulation, especially at the top of the pin, the simulation results still represent material flow well enough. This difference could be due to differences in tool position between experiment and simulation. In the simulation, the tool position is fixed at 60 mm from the top end of the workpiece. Meanwhile, during the experiment, the tool moved slightly past the end of the workpiece. When the tool is at that position, the LE tool does not touch the workpiece, so the heat input is reduced. This leads to circular extrusion not occurring and only extrusion in the direction of the welding speed. The presence of a defect in the form of a void in the area behind the pin strengthens this reason. When the tool moves forward, there will be a cavity behind it. This cavity will be filled with hot material, which will be extruded from front to back. When the material is not hot enough, the material will still be very “viscous” (high flow stress), so it cannot fill the cavity.

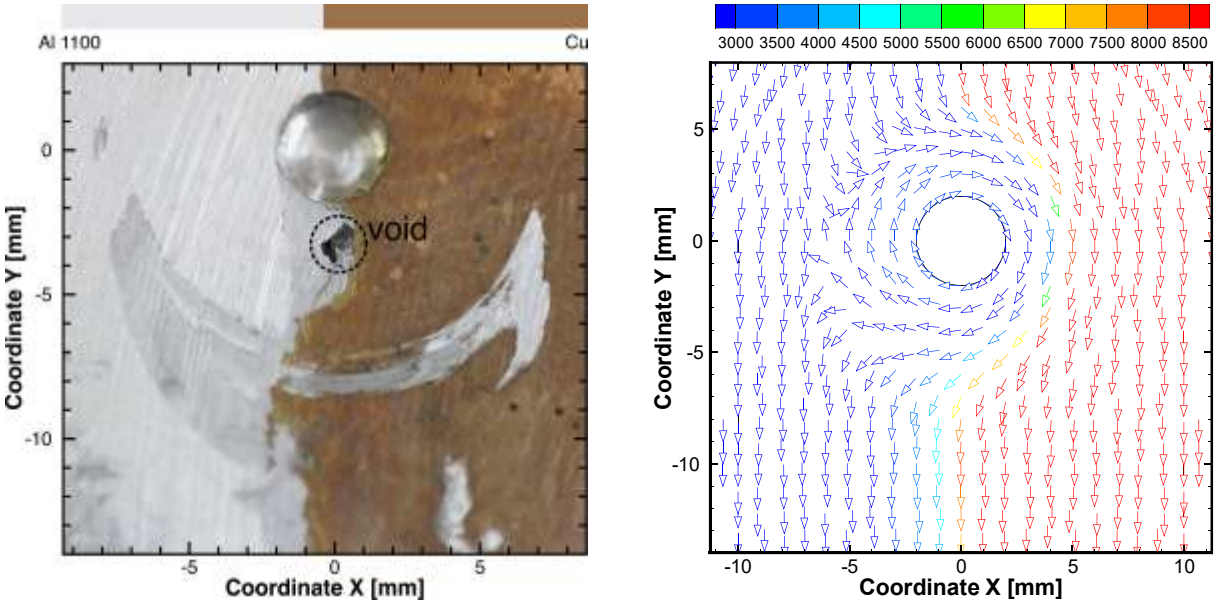

(a) (b)

Fig. 15. Top view (XY plane) results at Z = 2.5 mm for (a) experiment and (b) simulation which is colored by density

5. Conclusion

i) The workpiece yield strength and axial force from the tool affect the distribution of the convection coefficient at the workpiece-backing plate interface due to workpiece deformation.
ii) Based on temperature history, the convection coefficient distribution based on workpiece deformation generally matches the experimental results, outperforming uniform and temperature dependent.
iii) Higher peak temperature at the advancing side applies only near the heat source area because of tool relative velocity. However, material's thermal conductivity takes on the dominant factor as distance increases.
iv) With the help of tool axial pressure, the advancing side tends to extrude upward on the bottom surface of the workpiece, and the retreating side tends to extrude downward on the top surface of the workpiece with the help of tool axial pressure.
v) A cavity will be formed at the trailing edge when the material is not hot enough because of low heat input.

In this study, a simulation of the FSW process has been created using uniform, temperature, and deformation dependent to determine the distribution of convection coefficients at the bottom of the workpiece. Sufficient heat input is required to maintain the workpiece temperature enough to soften the material around the tool. Differences in material properties in dissimilar welding and heat input in AS and RS create a distinct temperature difference that will determine the weld quality. Low temperature leads to void defects due to insufficient flow in the stir zone. In contrast, excessive temperature tends to cause flash defects and reduces weld strength due to the overheating and material thinning effect. The convection coefficient distribution approach based on deformation can be considered feasible for a reference backing plate material design for future work. Thus, it will produce defect-free welds and have high weld strength efficiency.

Acknowledgment
This research was not funded by any grant.

References
[1] Rajendran, Ajith Raj, Mohammed Fahad, Dev Anand Manoharan, Azeem Hafiz Parayil Ajmal, Niaz Abdul Salam, and Jayaram Vijayan. "Investigation of Intermetallic Compound Formation in Dissimilar Metal Welds between Copper and Stainless Steel using Gas Tungsten Arc Welding." *Journal of Advanced Research in Applied Mechanics* 114, no. 1 (2024): 163-172. https://doi.org/10.37934/aram.114.1.163172

[2] Islam, M. R., M. Ishak, L. H. Shah, S. R. A. Idris, and C. Meriç. "Dissimilar welding of A7075-T651 and AZ31B alloys by gas metal arc plug welding method." *The International Journal of Advanced Manufacturing Technology* 88 (2017): 2773-2783. https://doi.org/10.1007/s00170-016-8993-6

[3] Raj, Sanjay, and Pankaj Biswas. "Experimental investigation of the effect of induction preheating on the microstructure evolution and corrosion behaviour of dissimilar FSW (IN718 and SS316L) joints." *Journal of Manufacturing Processes* 95 (2023): 143-159. https://doi.org/10.1016/j.jmapro.2023.04.021

[4] Xue, P., D. R. Ni, D. Wang, B. L. Xiao, and Z. Y. Ma. "Effect of friction stir welding parameters on the microstructure and mechanical properties of the dissimilar Al–Cu joints." *Materials science and engineering: A* 528, no. 13-14 (2011): 4683-4689. https://doi.org/10.1016/j.msea.2011.02.067

[5] Dhara, Sisir, and Abhishek Das. "Impact of ultrasonic welding on multi-layered Al–Cu joint for electric vehicle battery applications: A layer-wise microstructural analysis." *Materials Science and Engineering: A* 791 (2020): 139795. https://doi.org/10.1016/j.msea.2020.139795

[6] Feng, Ji, Xue Songbai, and Dai Wei. "Reliability studies of Cu/Al joints brazed with Zn–Al–Ce filler metals." *Materials & Design* 42 (2012): 156-163. https://doi.org/10.1016/j.matdes.2012.05.028

[7] Tavassolimanesh, Ahmad, and Ali Alavi Nia. "A new approach for manufacturing copper-clad aluminum bimetallic tubes by friction stir welding (FSW)." *Journal of Manufacturing Processes* 30 (2017): 374-384. https://doi.org/10.1016/j.jmapro.2017.10.010

[8] Darmadi, Djarot B., and Marco Talice. "Improving the strength of friction stir welded joint by double side friction welding and varying pin geometry." *Engineering Science and Technology, an International Journal* 24, no. 3 (2021): 637-647. https://doi.org/10.1016/j.jestch.2020.11.001

[9] He, Xiaocong, Fengshou Gu, and Andrew Ball. "A review of numerical analysis of friction stir welding." *Progress in Materials Science* 65 (2014): 1-66. https://doi.org/10.1016/j.pmatsci.2014.03.003

[10] Dialami, Narges, Michèle Chiumenti, M. Cervera, A. Segatori, and W. Osikowicz. "Enhanced friction model for Friction Stir Welding (FSW) analysis: Simulation and experimental validation." *International Journal of Mechanical Sciences* 133 (2017): 555-567. https://doi.org/10.1016/j.ijmecsci.2017.09.022

[11] Chen, Jie, Xue Wang, Lei Shi, Chuansong Wu, Huijie Liu, and Gaoqiang Chen. "Numerical simulation of weld formation in friction stir welding based on non-uniform tool-workpiece interaction: An effect of tool pin size." *Journal of Manufacturing Processes* 86 (2023): 85-97. https://doi.org/10.1016/j.jmapro.2022.12.052

[12] Santosa, I. Dewa Made Cipta, I. Gede Nyoman Suta Waisnawa, Putu Wijaya Sunu, I. Wayan Temaja, and Liang Li. "CFD Air Flow Evaluation of Finned Tube Evaporator for Refrigerated Display Cabinet Application." *CFD Letters* 16, no. 9 (2024): 52-63. https://doi.org/10.37934/cfdl.16.9.5263

[13] Bindu, M. D., P. S. Tide, and A. B. Bhasi. "Numerical Studies on Temperature and Material Flow During Friction Stir Welding using Different Tool Pin Profiles." *Journal of Advanced Research in Fluid Mechanics and Thermal Sciences* 83, no. 1 (2021): 91-104. https://doi.org/10.37934/arfmts.83.1.91104

[14] Larsen, Anders, Mathias Stolpe, and Jesper Henri Hattel. "Estimating the workpiece-backing plate heat transfer coefficient in friction stirwelding." *Engineering Computations: International Journal for Computer-Aided Engineering and Software* 29, no. 1 (2012): 65-82. https://doi.org/10.1108/02644401211190573

[15] Meyghani, Bahman, Mokhtar Awang, and C. S. Wu. "Finite element modeling of friction stir welding (FSW) on a complex curved plate." *Journal of Advanced Joining Processes* 1 (2020): 100007. https://doi.org/10.1016/j.jajp.2020.100007

[16] Nandan, R., T. J. Lienert, and T. DebRoy. "Toward reliable calculations of heat and plastic flow during friction stir welding of Ti-6Al-4V alloy." *International Journal of Materials Research* 99, no. 4 (2008): 434-444. https://doi.org/10.3139/146.101655

[17] Rosochowska, M., K. Chodnikiewicz, and R. Balendra. "A new method of measuring thermal contact conductance." *Journal of materials processing technology* 145, no. 2 (2004): 207-214. https://doi.org/10.1016/S0924-0136(03)00671-X

[18] Hasan, Mohammed M., M. Ishak, and M. R. M. Rejab. "Effect of backing material and clamping system on the tensile strength of dissimilar AA7075-AA2024 friction stir welds." *The International Journal of Advanced Manufacturing Technology* 91 (2017): 3991-4007. https://doi.org/10.1007/s00170-017-0033-7

[19] Krishnan, Girish, and Ankur Jain. "Transient temperature distribution in a multilayer semiconductor device with dynamic thermal load and non-uniform thermal contact resistance between layers." *International Journal of Heat and Mass Transfer* 214 (2023): 124374. https://doi.org/10.1016/j.ijheatmasstransfer.2023.124374

[20] Gilmore, David G., ed. *Spacecraft thermal control handbook: cryogenics*. Vol. 2. Aiaa, 2002.

[21] An, Ben, Linxue An, Yuping Huang, Jiaqi Li, Ben Guan, and Rui Li. "The influence of surface topography on thermal contact resistance of 7075-T6/beryllium bronze." *Thermal Science and Engineering Progress* 46 (2023): 102196. https://doi.org/10.1016/j.tsep.2023.102196

[22] Upadhyay, Piyush, and Anthony P. Reynolds. "Effects of forge axis force and backing plate thermal diffusivity on FSW of AA6056." *Materials Science and Engineering: A* 558 (2012): 394-402. https://doi.org/10.1016/j.msea.2012.08.018

[23] Kulkarni, B. S., S. B. Pankade, S. R. Andhale, and C. L. Gogte. "Effect of backing plate material diffusivity on microstructure, mechanical properties of friction stir welded joints: a review." *Procedia Manufacturing* 20 (2018): 59-64. https://doi.org/10.1016/j.promfg.2018.02.008

[24] Choi, Woong Jo, Justin D. Morrow, Frank E. Pfefferkorn, and Michael R. Zinn. "The effects of welding parameters and backing plate diffusivity on energy consumption in friction stir welding." *Procedia Manufacturing* 10 (2017): 382-391. https://doi.org/10.1016/j.promfg.2017.07.011

[25] Imam, Murshid, Vikranth Racherla, and Kajal Biswas. "Effect of backing plate material in friction stir butt and lap welding of 6063-T4 aluminium alloy." *The International Journal of Advanced Manufacturing Technology* 77 (2015): 2181-2195. https://doi.org/10.1007/s00170-014-6617-6

[26] Kulkarni, Bhardwaj, and Sandeep Pankade. "Effects of different backing plates and tool design on the flash defect developed during friction stir welding of AA6061 aluminium alloy." (2022). https://doi.org/10.21203/rs.3.rs-1968882/v1

[27] Flint, T. F., J. A. Francis, and M. C. Smith. "A semi-analytical solution for the transient temperature field generated by a volumetric heat source developed for the simulation of friction stir welding." *International Journal of Thermal Sciences* 138 (2019): 586-595. https://doi.org/10.1016/j.ijthermalsci.2018.12.049

[28] Khodir, Saad Ahmed, Toshiya Shibayanagi, and Masaaki Naka. "Control of hardness distribution in friction stir welded AA2024-T3 aluminum alloy." *Materials transactions* 47, no. 6 (2006): 1560-1567. https://doi.org/10.2320/matertrans.47.1560

[29] Upadhyay, Piyush, and Anthony Reynolds. "Effect of backing plate thermal property on friction stir welding of 25-mm-thick AA6061." *Metallurgical and Materials Transactions A* 45 (2014): 2091-2100. https://doi.org/10.1007/s11661-013-2121-0

[30] Kah, Paul, Richard Rajan, Jukka Martikainen, and Raimo Suoranta. "Investigation of weld defects in friction-stir welding and fusion welding of aluminium alloys." *International Journal of Mechanical and Materials Engineering* 10 (2015): 1-10. https://doi.org/10.1186/s40712-015-0053-8

[31] Shankar, Sachindra, Pedro Vilaça, Priyabrat Dash, Somnath Chattopadhyaya, and Sergej Hloch. "Joint strength evaluation of friction stir welded Al-Cu dissimilar alloys." *Measurement* 146 (2019): 892-902. https://doi.org/10.1016/j.measurement.2019.07.019

[32] Sheppard, T., and D. S. Wright. "Determination of flow stress: Part 1 constitutive equation for aluminium alloys at elevated temperatures." *Metals Technology* 6, no. 1 (1979): 215-223. https://doi.org/10.1179/030716979803276264

[33] Yang, C. L., C. S. Wu, and X. Q. Lv. "Numerical analysis of mass transfer and material mixing in friction stir welding of aluminum/magnesium alloys." *Journal of Manufacturing Processes* 32 (2018): 380-394. https://doi.org/10.1016/j.jmapro.2018.03.009

[34] Anwari, Muhammad Izhar Hishyam, Nor Afzanizam Samiran, Izuan Amin Ishak, and Muhammad Suhail Sahul Hamid. 2024. "CFD Modelling of Plasma Downdraft Coal Gasification Process: Effect of Throat Diameter on the Produced Syngas Composition". *Journal of Advanced Research in Numerical Heat Transfer* 22 (1):14-30. https://doi.org/10.37934/arnht.22.1.1430

[35] Nandan, R., B. Prabu, A. De, and T. Debroy. "Improving reliability of heat transfer and materials flow calculations during friction stir welding of dissimilar aluminum alloys." *WELDING JOURNAL-NEW YORK*- 86, no. 10 (2007): 313.

[36] Cho, Hoon-Hwe, Sung-Tae Hong, Jae-Hun Roh, Hyun-Sik Choi, Suk Hoon Kang, Russell J. Steel, and Heung Nam Han. "Three-dimensional numerical and experimental investigation on friction stir welding processes of ferritic stainless steel." *Acta Materialia* 61, no. 7 (2013): 2649-2661. https://doi.org/10.1016/j.actamat.2013.01.045

[37] Standard, A. S. T. M. "Standard test methods for tension testing of metallic materials." *ASTM International: West Conshohocken, PA, USA* (2013). https://doi.org/10.1520/e0008_e0008m-13a
[38] Darmadi, Djarot B. "Incorporating Aged Martensite Model in Residual Stress Prediction of Ferritic Steels Girth Weld." *FME Transactions* 47, no. 4 (2019). https://doi.org/10.5937/fmet1904901D
[39] Jagadeesha, C. B. "Flow analysis of materials in friction stir welding." *Journal of the Mechanical Behavior of Materials* 27, no. 3-4 (2018): 20180020. https://doi.org/10.1515/jmbm-2018-0020
[40] Colligan, K. "Material flow behavior during friction welding of aluminum." *Weld J* 75, no. 7 (1999): 229s-237s.
[41] Krishnan, K. N. "On the formation of onion rings in friction stir welds." *Materials science and engineering: A* 327, no. 2 (2002): 246-251. https://doi.org/10.1016/S0921-5093(01)01474-5